eLIFE
elifesciences.org

Figures and figure supplements

Fatty acid remodeling by LPCAT3 enriches arachidonate in phospholipid membranes and regulates triglyceride transport

Tomomi Hashidate-Yoshida, et al.

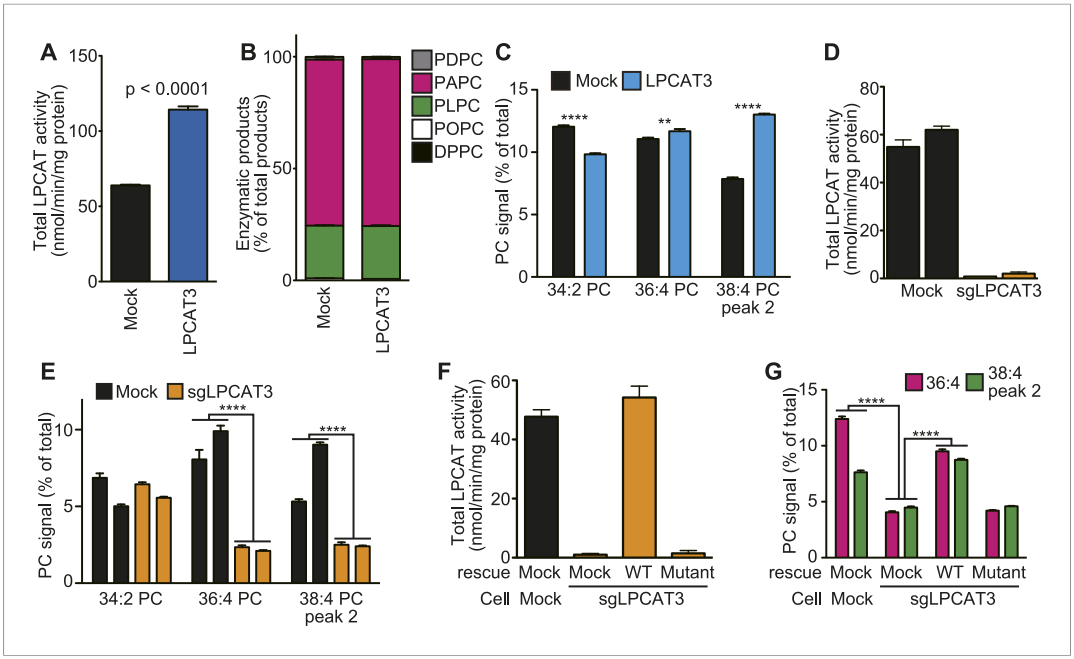

Figure 1. LPCAT3 regulates arachidonate levels in PC. (**A** and **B**) LPCAT activity and selectivity in mock- or LPCAT3-overexpressing RH 7777 cells. LPC and five acyl-CoA species (16:0-, 18:1-, 18:2-, 20:4-, and 22:6-CoA) were used as substrates of LPCAT assay to generate DPPC (16:0–16:0 PC), POPC (16:0–18:1 PC), PLPC (16:0–18:2 PC), PAPC (16:0–20:4 PC), and PDPC (16:0–22:6 PC). The total of five products (**A**) and the relative amount of each PC species, equivalent to acyl-CoA selectivity (**B**) are shown. The experiment was performed in technical triplicate. (**C**) Levels of selected PC species in mock- or LPCAT3-stable cells (n = 8). Data are % of the total signals from all PC species detected. (**D**–**G**) Total LPCAT activity products (**D** and **F**, in technical triplicate) and PC levels of the selected species (**E** (n = 3) and **G** (n = 5)) were measured in mock- or LPCAT3-null RH 7777 cells (**D** and **E**) or the null cells rescued with LPCAT3 or a mutant lacking activity (**F** and **G**). (**D** and **E**) The results of two different clones are separately indicated. Error bars are SD (**A**, **B**, **D**, and **F**) or SEM (**C**, **E**, and **G**). sgLPCAT3: single guide RNA targeting *Lpcat3*. **p < 0.01, ****p < 0.0001. See also ***Figure 1—figure supplements 1–3***.

DOI: 10.7554/eLife.06328.003

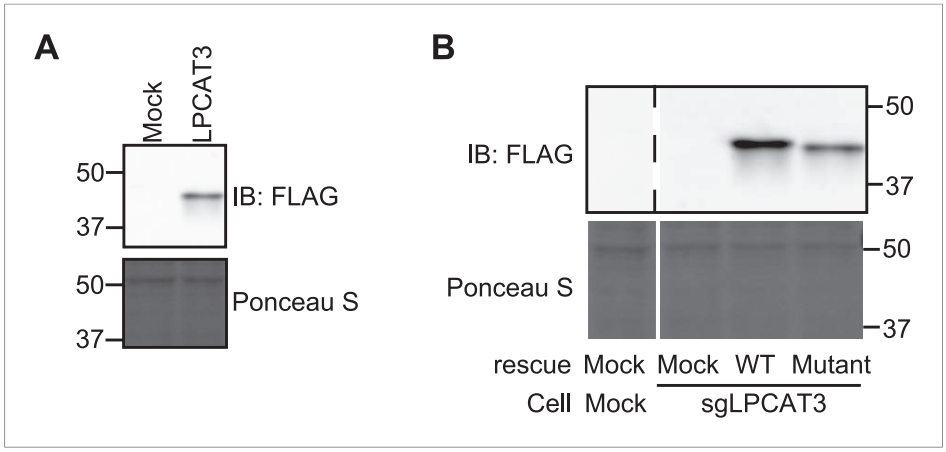

Figure 1—figure supplement 1. Confirmation of stable expression. (**A** and **B**) Stable overexpression of transfected FLAG-LPCAT3 was detected by western blot analysis using an anti-FLAG antibody. Ponceau S staining was used as a loading control. (**A**) Detection of FLAG-LPCAT3 in RH 7777 cells. (**B**) Detection of wild type FLAG-LPCAT3 or a H374A mutant lacking activity. The parental cells are LPCAT3-null RH 7777 cells. Control cells that were stably transfected with an empty vector were also established.

DOI: 10.7554/eLife.06328.004

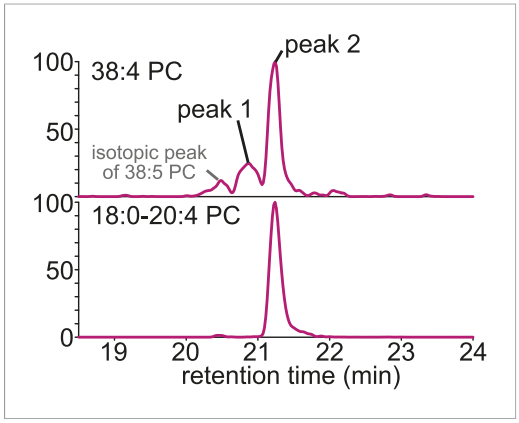

Figure 1—figure supplement 2. Annotation of LC-MS signals. Using methods that detect head group information at Q3 (top, in this case, 38:4 PC is detected using a precursor scan of *m/z* 184.1, a characteristic fragment of PC) multiple peaks that might have different combinations of *sn*-1 and *sn*-2 fatty acids (e.g., 16:0–22:4 PC, 18:0–20:4 PC, or 18:1–20:3 PC) can be detected with different retention times. When fatty acid fragments are selected at Q3 (bottom, in this case, a stearate fragment of 38:4 PC is selected at Q3 using SRM), the peaks can be attributed to a single acyl-chain combination (since stearate is detected, only 18:0–20:4 PC is detected). By comparing the retention times of the two chromatograms, we can estimate the acyl-chain composition of phospholipids eluted differently (in this case, peak 2 of 38:4 PC is annotated as 18:0–20:4 PC).

DOI: 10.7554/eLife.06328.005

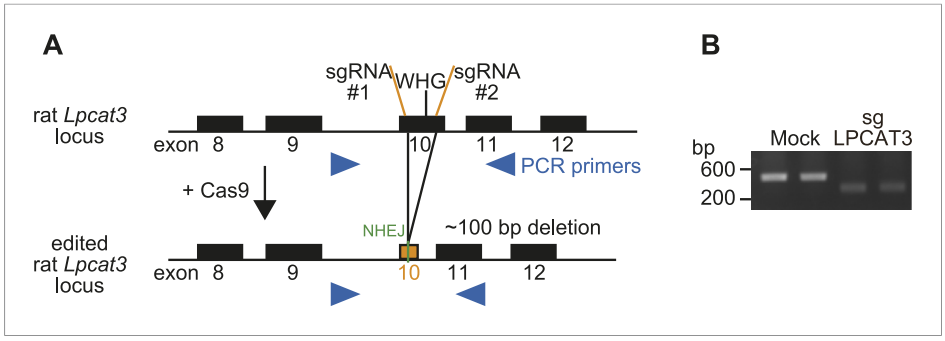

Figure 1—figure supplement 3. Generation of LPCAT3-null cells. (**A**) Strategy for genome editing of rat *Lpcat3* locus using the CRISPR/Cas9 system. The WHG sequence required for LPCAT3 activity was removed by cleavage of two adjacent regions, leading to a small genomic deletion. Arrowheads: PCR primers for analysis of deletion; sgRNA: single guide RNA; NHEJ: non-homologous end joining. (**B**) Genome editing of *Lpcat3* in RH 7777 cells was confirmed by PCR.

DOI: 10.7554/eLife.06328.006

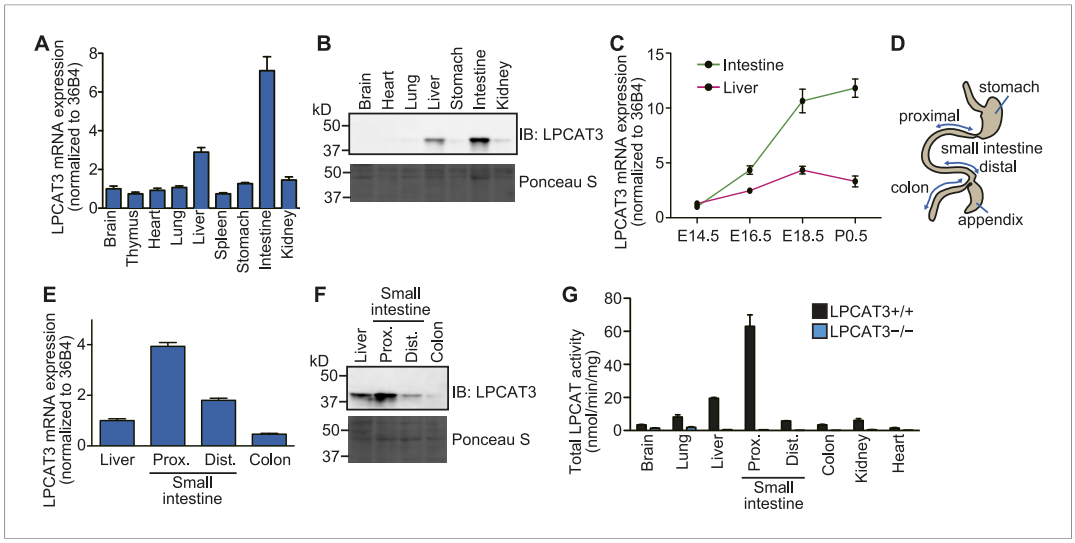

Figure 2. Tissue distribution of LPCAT3. (**A**–**F**) The distribution of LPCAT3 mRNA (**A**, **C**, and **E**, by quantitative PCR) or protein (**B** and **F**, by western blot analysis) was analyzed in different tissues at E18.5 (**A**, **B**, **E**, and **F**) or at various perinatal stages (**C**). Ponceau S staining was performed as a loading control for western blot analysis. (**D**) Illustration of the intestine separated into the proximal-, distal small intestine, and colon. (**G**) LPCAT activity was determined in tissues obtained from mice of the indicated genotype at E18.5. See legend of ***Figure 1A*** for description of the method. Error bars are SEM (n = 3). See also ***Figure 2—figure supplement 1***.

DOI: 10.7554/eLife.06328.007

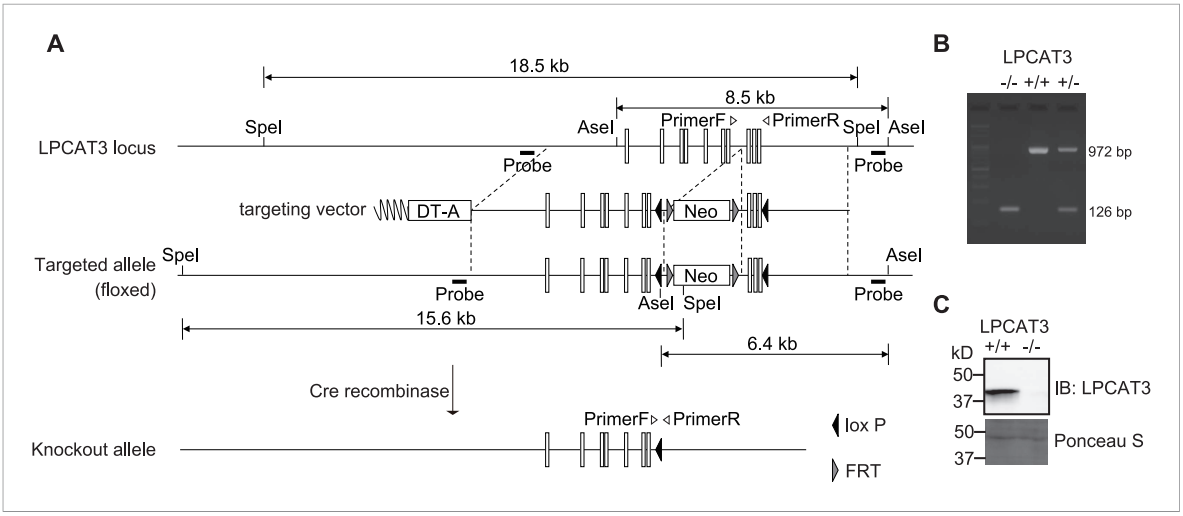

Figure 2—figure supplement 1. Generation of LPCAT3-deficient mice. (**A**) Strategy for gene targeting to generate LPCAT3-deficient mice and for the identification of targeted clones. Neo: Neomycin-resistance cassette; DT-A: diphtheria toxin subunit A cassette. (**B** and **C**) LPCAT3 deficiency was confirmed by PCR using tail tip genomic DNA (**B**) and by western blot analysis of proteins from small intestine (**C**).
DOI: 10.7554/eLife.06328.008

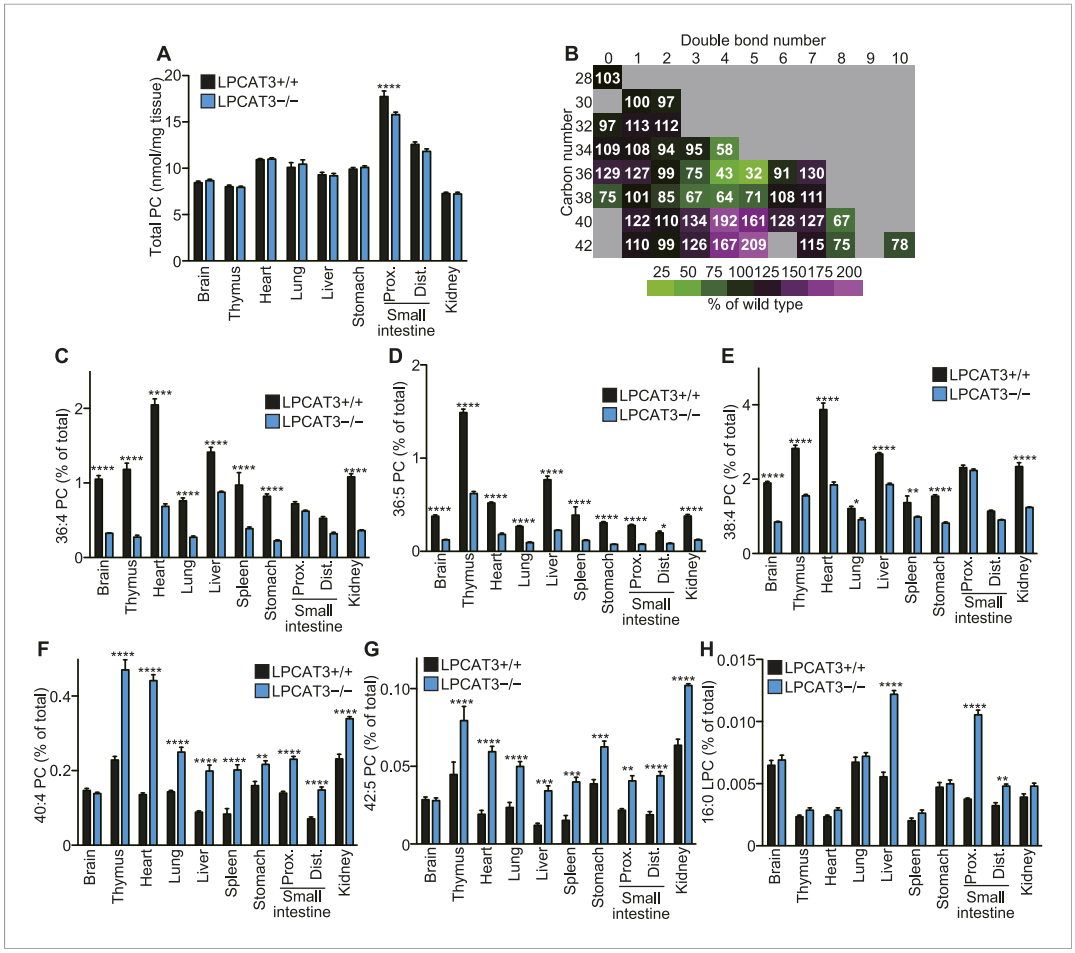

Figure 3. LPCAT3 regulates PC arachidonate levels in vivo. Lipidomics analyses were performed in various tissues of mice at E18.5. (**A**) Total PC amounts in tissues from wild type and LPCAT3-deficient mice. (**B**) Heat map showing the ratio of each PC species in LPCAT3-deficient mice. Each value is the average of ratio values (% of wild type) for tissues analyzed in (**C**–**H**). (**C**–**G**) The levels of the indicated PC species in wild type and LPCAT3-deficient mice were measured by LC-MS. (**H**) The levels of 16:0 LPC were measured in wild type and LPCAT3-deficient mice. Data were normalized to total MS signals shown in ***Figure 3—figure supplement 1***. Prox.: Proximal; Dist.: Distal. (**A**, and **C**–**H**) Error bars are SEM (n = 5). *p < 0.05, **p < 0.01, ***p < 0.001, ****p < 0.0001. See also ***Figure 3—figure supplements 1, 2***.

DOI: 10.7554/eLife.06328.009

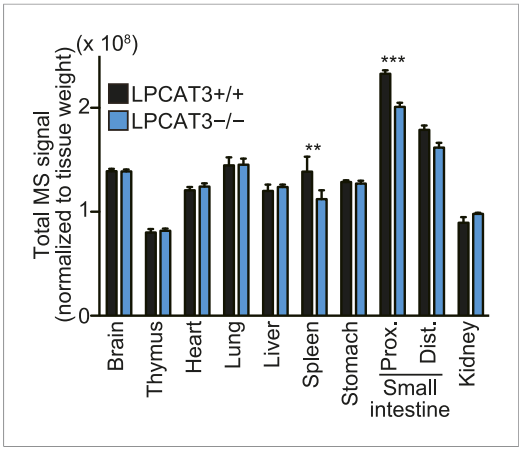

Figure 3—figure supplement 1. Total signals used for normalization of lipidomic profiling analysis. Total MS signals from all the SRM channels of the lipidomic profiling analysis, which were used for normalization (n = 5). Note that the amount of spleen lipids analyzed was not normalized to tissue weight, making if difficult to compare the total values (see 'Materials and methods').
DOI: 10.7554/eLife.06328.010

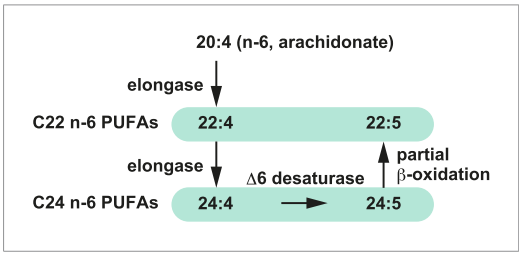

Figure 3—figure supplement 2. Metabolism of arachidonate. Metabolism of arachidonate (elongation, desaturation, and partial β-oxidation) that might have been enhanced due to the excess of arachidonoyl-CoA in LPCAT3-deficient mice.
DOI: 10.7554/eLife.06328.011

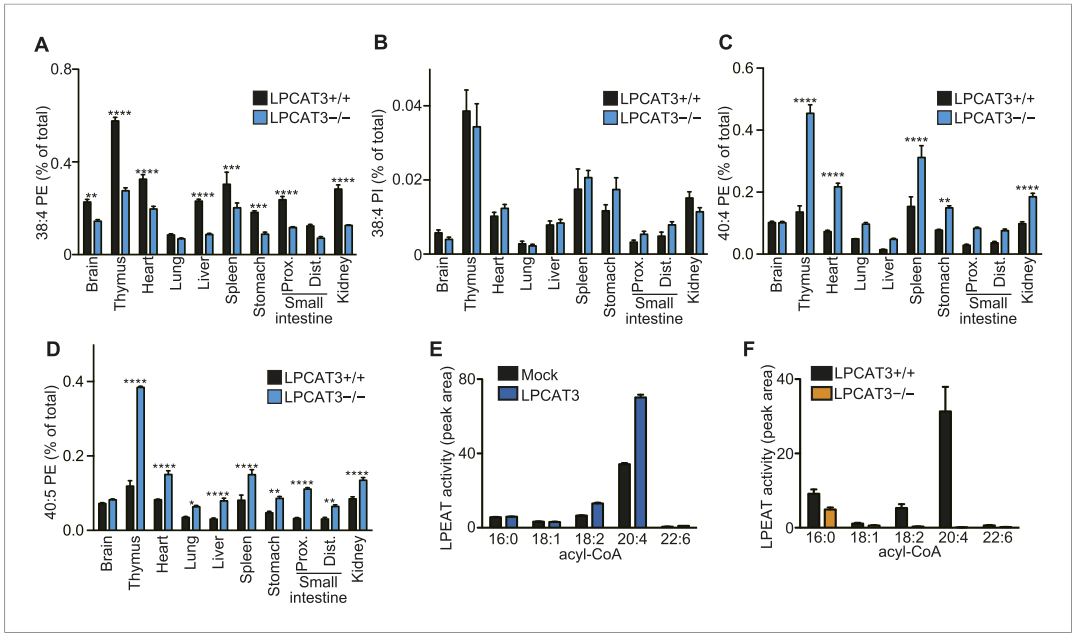

Figure 4. LPCAT3 regulates PE arachidonate levels in vivo. (**A**–**D**) The levels of the indicated PE species in wild type and LPCAT3-deficient mice were measured by LC-MS and normalized using the values in ***Figure 3—figure supplement 1***. Error bars are SEM (n = 5). (**E** and **F**) LPEAT activity was examined in mock- or LPCAT3-transfected RH 7777 cells (error bars are SD, technical triplicate) (**E**) and proximal small intestine from wild type or LPCAT3-deficient mice (error bars are SEM, n = 3) (**F**). 17:1 LPE was used instead of LPC in a similar experiment to ***Figure 1A***, and peak areas of each LPEAT product are illustrated. Prox.: Proximal; Dist.: Distal. *p < 0.05, **p < 0.01, ***p < 0.001, ****p < 0.0001.

DOI: 10.7554/eLife.06328.013

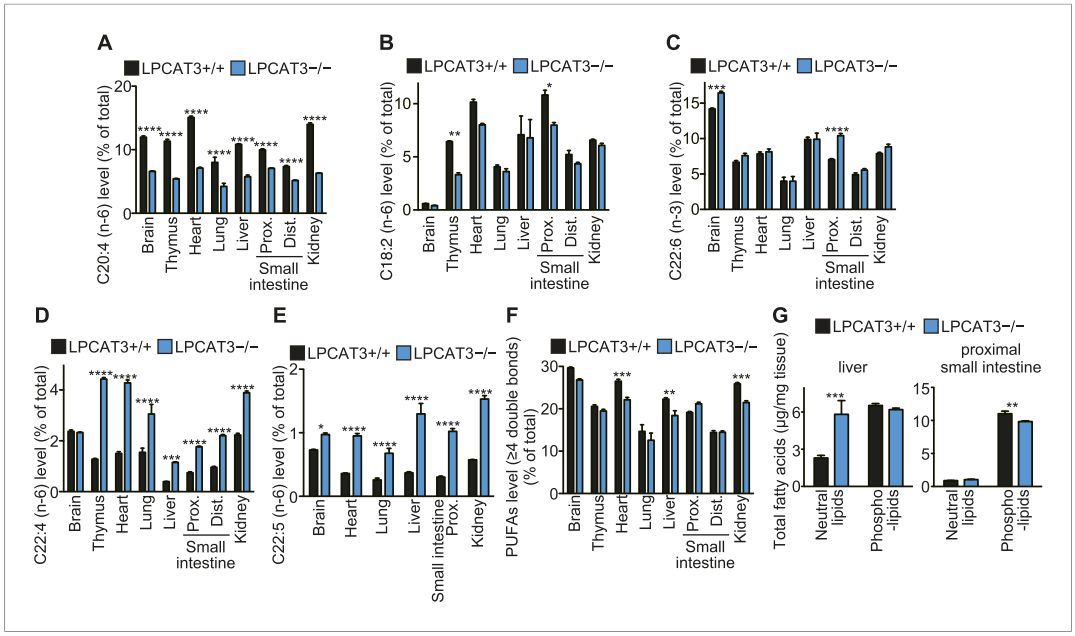

Figure 5. Arachidonate levels and metabolism are changed in LPCAT3-deficient mice GC-FID was performed using various tissues to analyze fatty acid amounts and compositions in total lipids, as well as those of lipid subclasses. (**A**–**F**) The levels of the indicated PUFAs (**A**–**E**), and the total of PUFAs (**F**, sum of PUFAs with four or more double bonds) in wild type and LPCAT3-deficient mice were measured by GC-FID. Data are % of the total levels shown in ***Figure 5—figure supplement 1***. (**G**) The total amounts of fatty acids in neutral lipids and phospholipids that were fractionated from the indicated tissues in wild type and LPCAT3-deficient mice were analyzed by GC-FID. Prox.: Proximal; Dist.: Distal. Error bars are SEM (n = 5). *p < 0.05, **p < 0.01, ***p < 0.001, ****p < 0.0001. See also ***Figure 5—figure supplement 1***.

DOI: 10.7554/eLife.06328.015

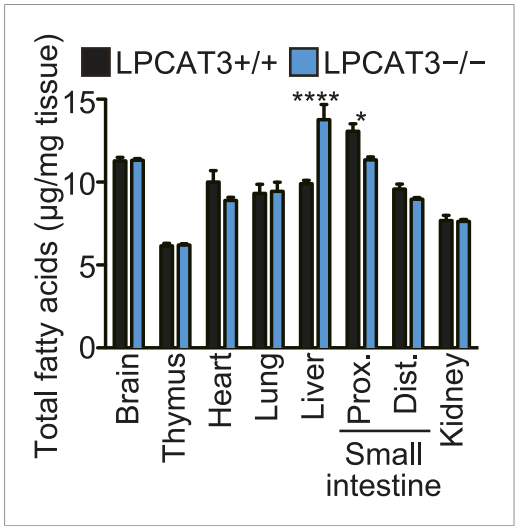

Figure 5—figure supplement 1. Total fatty acids in tissues. Total signals from GC-FID analyses that were used for normalization in ***Figure 5A–F***.

DOI: 10.7554/eLife.06328.016

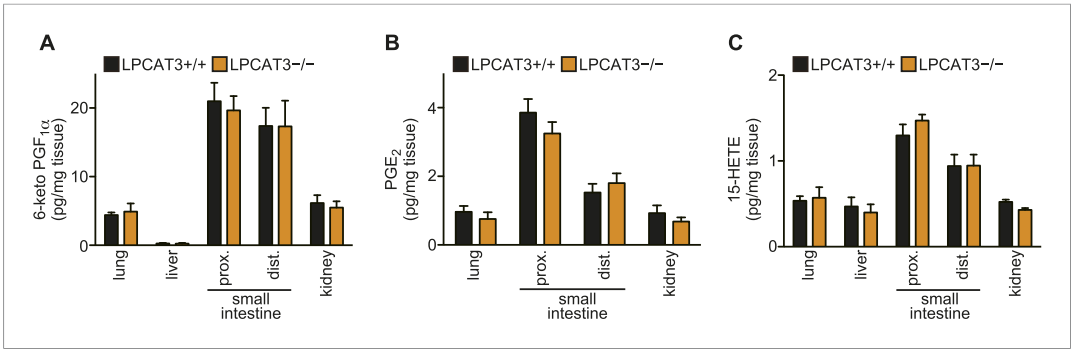

Figure 6. Eicosanoid levels are not affected in tissues of LPCAT3-deficient mice. (**A**–**C**) The levels of 6-keto $PGF_1\alpha$ (**A**), PGE_2 (**B**) and 15-HETE (**C**) in wild type and LPCAT3-deficient mice at E18.5. Error bars are SEM (n = 5). PG: prostaglandin; HETE: hydroxyeicosatetraenoic acid.

DOI: 10.7554/eLife.06328.017

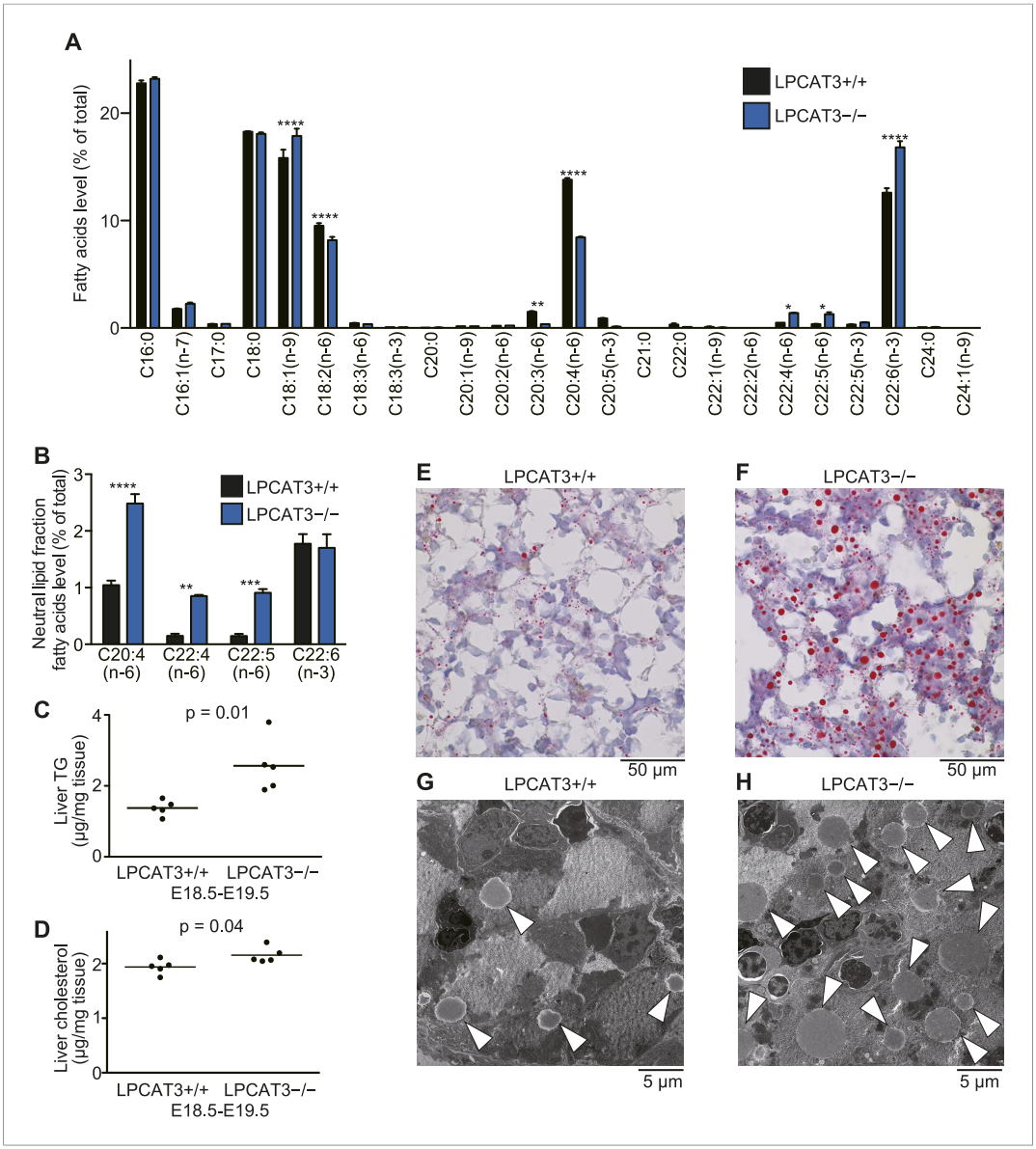

Figure 7. TGs accumulate in the embryonic liver of LPCAT3-deficient mice. (**A** and **B**) Liver phospholipids (**A**) and neutral lipids (**B**, only selected PUFAs are shown) were obtained by solid-phase extraction and used for the analysis of acyl-chain composition using wild type and LPCAT3-deficient mice. The percentage of fatty acids detected by GC-FID is illustrated. Error bars are SEM (n = 5). (**C** and **D**) Levels of TG (**C**) and cholesterol (**D**) in liver were measured using wild type and LPCAT3-deficient mice at E18.5–E19.5. (**E**–**H**) The amounts of lipid droplets in liver of wild type and LPCAT3-deficient mice at E18.5–E19.5 were detected by oil red O and hematoxylin staining (**E** and **F**), or by electron microscopy (**G** and **H**). Arrowheads: lipid droplets. *p < 0.05, **p < 0.01, ****p < 0.0001. See also ***Figure 7—figure supplements 1, 2***.

DOI: 10.7554/eLife.06328.018

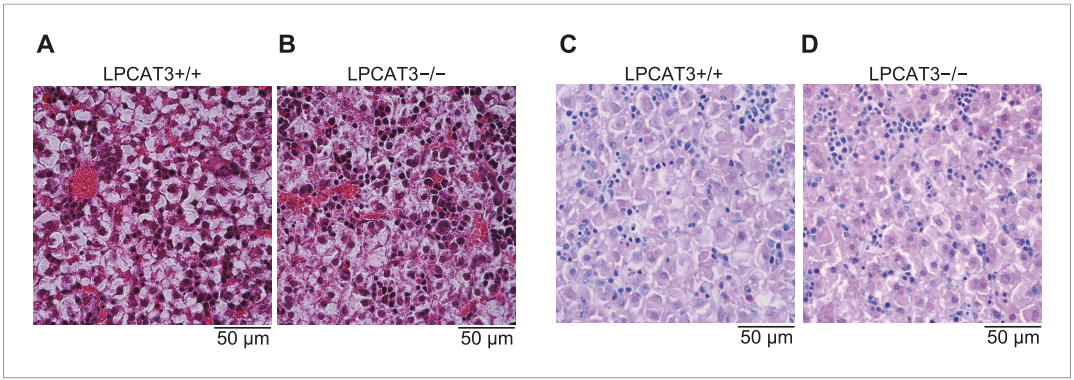

Figure 7—figure supplement 1. Histological analysis of embryonic liver. (**A**–**D**) Histological images of liver sections from wild type and LPCAT3-deficient mice at E18.5–E19.5 stained by hematoxylin/eosin (**A** and **B**) or PAS/hematoxylin (**C** and **D**).

DOI: 10.7554/eLife.06328.019

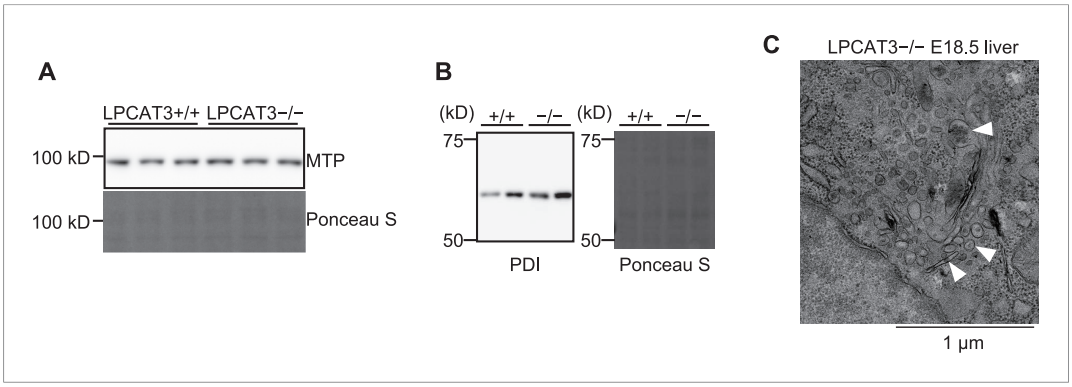

Figure 7—figure supplement 2. The machinery for VLDL assembly is present in LPCAT3-deficient liver. (**A** and **B**) The protein expression levels of MTP (**A**) and PDI (**B**) in liver of wild type and LPCAT3-deficient mice at E18.5–E19.5 were examined by western blot. Ponceau S staining was used as a loading control. (**C**) VLDL-like particles (arrowhead) were detected in the Golgi apparatus of hepatocytes in LPCAT3-deficient mice at E18.5–E19.5, showing that VLDL assembly is not absent.

DOI: 10.7554/eLife.06328.020

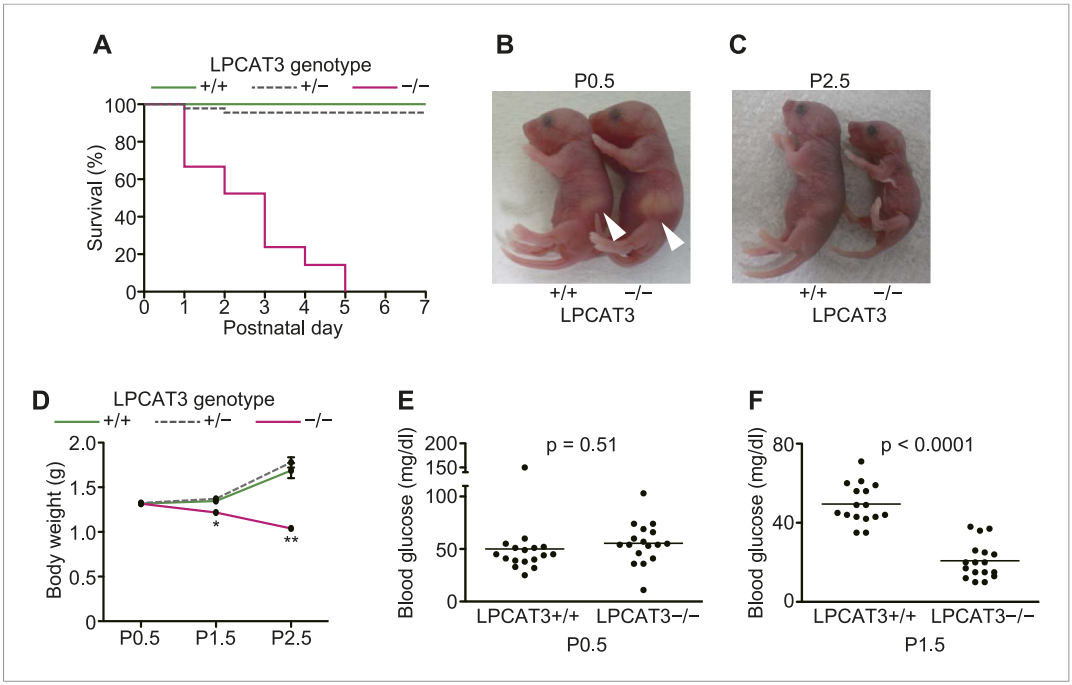

Figure 8. LPCAT3-deficient mice are neonatally lethal. (**A**–**D**) The survival rate (**A**), gross appearance (**B** and **C**), and body weight change (n = 9–62) (**D**) were evaluated in neonatal mice of the indicated genotypes. Arrowhead: normal milk intake in both genotypes. (**E** and **F**) Blood glucose was measured in wild type and LPCAT3-deficient mice at P0.5 (**E**) and P1.5 (**F**). Error bars are SEM. *p < 0.05, **p < 0.01. See also ***Figure 8—figure supplement 1***.

DOI: 10.7554/eLife.06328.021

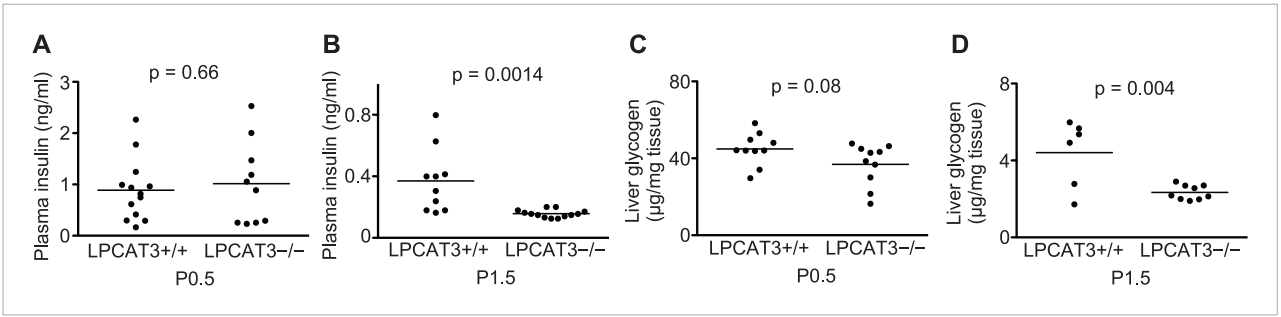

Figure 8—figure supplement 1. Plasma insulin and liver glycogen in LPCAT3-deficient mice. (**A**–**D**) Plasma insulin (**A** and **B**) and liver glycogen (**C** and **D**) were measured in wild type and LPCAT3-deficient mice at P0.5 and P1.5. Notice that insulin is not higher in LPCAT3-deficient mice than in wild type mice, and that liver glycogen levels are reduced at P1.5 in both genotypes.

DOI: 10.7554/eLife.06328.022

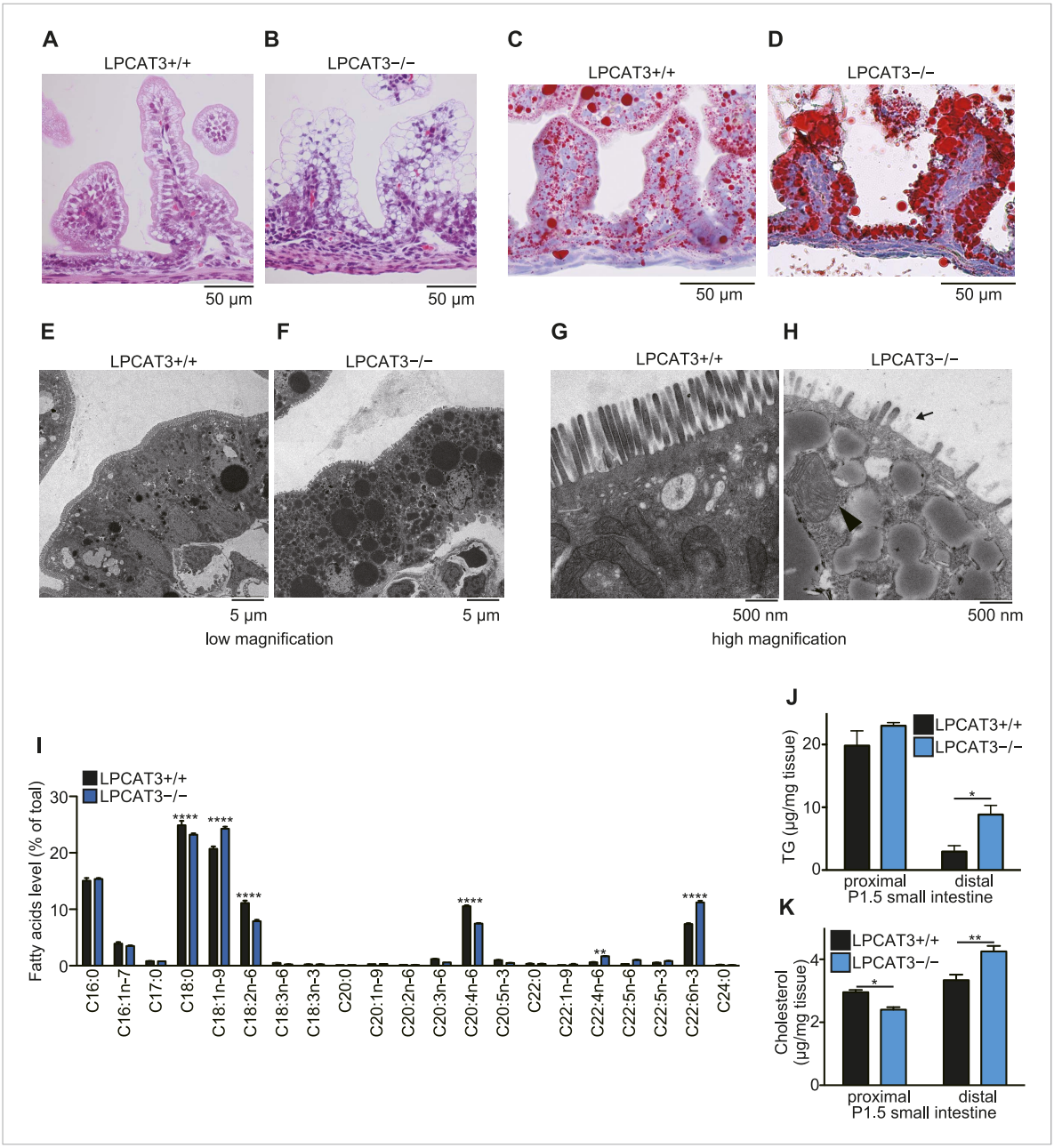

Figure 9. TG accumulation in enterocytes of LPCAT3-deficient mice. (**A**–**H**) Histology of the proximal small intestine of mice at P1.5 was analyzed by light microscopy after staining with hematoxylin and eosin (**A** and **B**), oil red O and hematoxylin (**C** and **D**), or by electron microscopy (**E**–**H**). (**H**) Shortened microvilli (arrow) and a mitochondrion with disrupted outer membrane (arrowhead) are seen in LPCAT3-deficient mice. (**I**) Phospholipids from proximal small intestine were obtained by solid-phase extraction and used for the analysis of acyl-chain composition using wild type and LPCAT3-deficient mice. The percentage of fatty acids detected by GC-FID is illustrated. (**J** and **K**) Levels of TG (**J**) and cholesterol (**K**) in small intestine samples from wild type and LPCAT3-deficient mice at P1.5. Error bars are SEM (n = 5). *p < 0.05, **p < 0.01. See also ***Figure 9—figure supplements 1, 2***.

DOI: 10.7554/eLife.06328.023

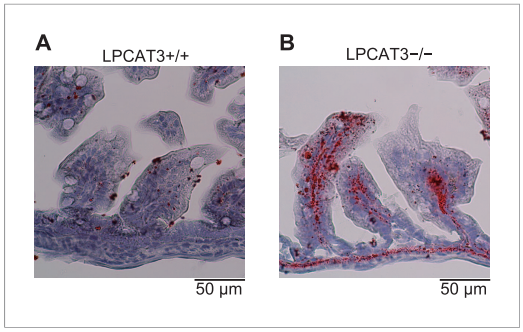

Figure 9—figure supplement 1. Distal small intestine of LPCAT3-deficient mice absorbs lipids. (**A** and **B**) Oil red O/hematoxylin staining of distal small intestine from wild type (**A**) and LPCAT3-deficient mice (**B**) at P1.5.
DOI: 10.7554/eLife.06328.024

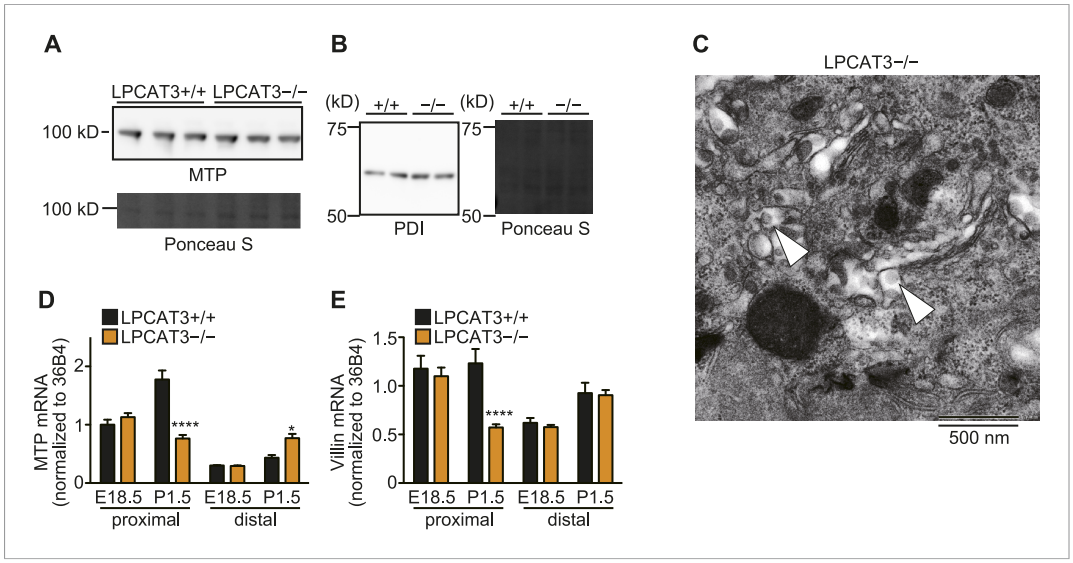

Figure 9—figure supplement 2. The machinery for chylomicron assembly is present in LPCAT3-deficient mice. (**A** and **B**) The protein levels of MTP (**A**) and PDI (**B**) were examined in proximal small intestine of wild type and LPCAT3-deficient mice at E18.5–E19.5 by western blot analysis. Ponceau S staining was used as a loading control. (**C**) Chylomicron-like particles (arrowheads) were detected in the Golgi apparatus of enterocytes from the proximal small intestine of LPCAT3-deficient mice at P0.5, showing that chylomicron assembly is not absent. (**D** and **E**) MTP (**D**) and villin (**E**) mRNA levels were quantified in small intestine of wild type and LPCAT3-deficient mice at E18.5–E19.5 or P1.5 by quantitative PCR (n = 6). Error bars are SEM. *p < 0.05, **p < 0.01, ****p < 0.0001.
DOI: 10.7554/eLife.06328.025

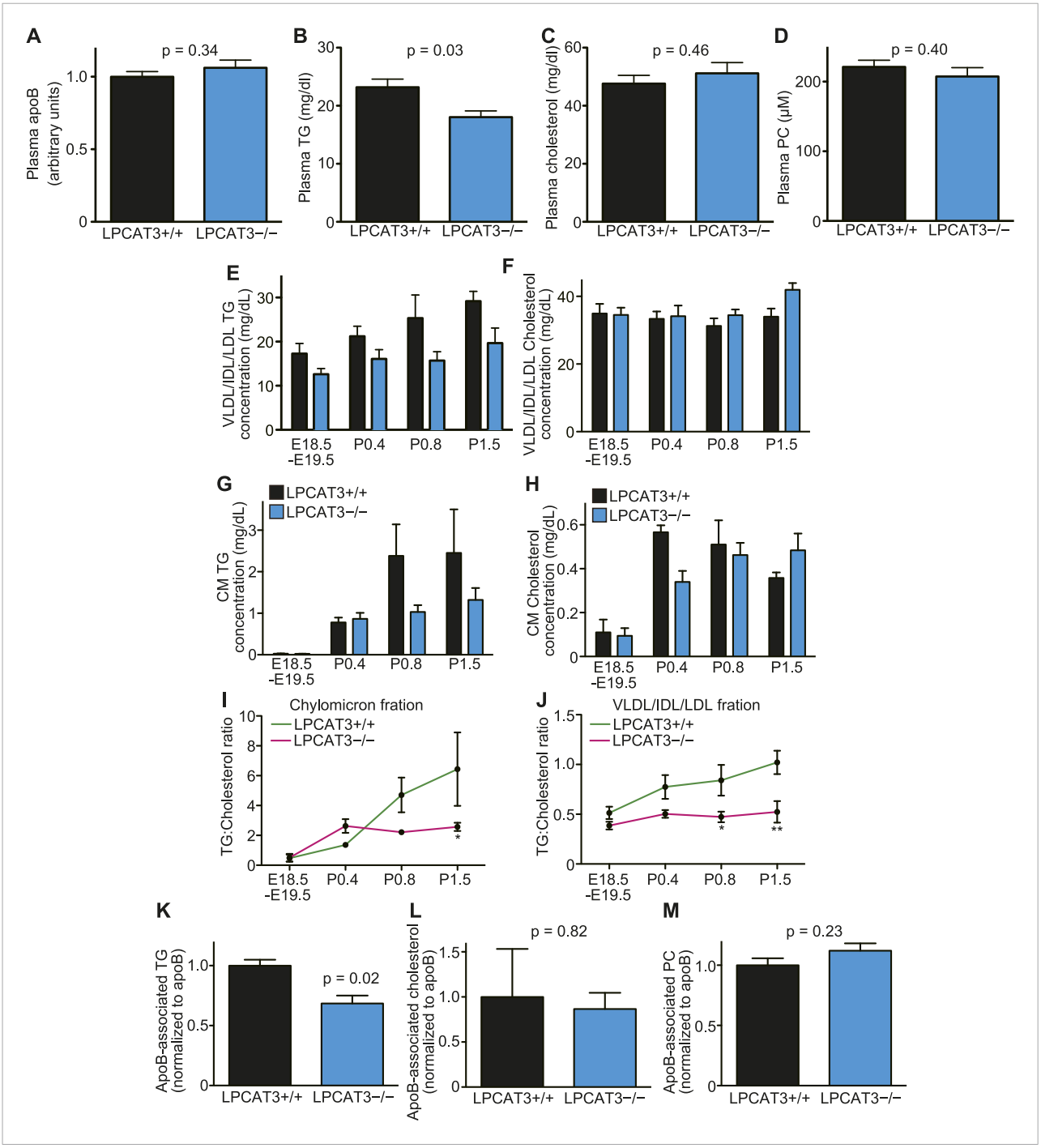

Figure 10. The levels of TGs are decreased in plasma lipoproteins of LPCAT3-deficient mice. (**A**–**D**) The levels of apoB (**A**), TG (**B**), cholesterol (**C**), and PC (**D**) were measured in plasma of wild type and LPCAT3-deficient mice at E18.5–E19.5 (n = 10). (**E**–**J**) Plasma lipoproteins from wild type and LPCAT3-deficient mice were fractionated by gel-filtration chromatography (n = 5). TG (**E** and **G**) and cholesterol (**F** and **H**) levels in VLDL/IDL/LDL fractions (**E** and **F**) or chylomicron fractions (**G** and **H**) were calculated from the raw data shown in ***Figure 10—figure supplements 1–H***. The differences in (**E**) did not reach statistical significance, but the changes in some subfractions in the raw data were significant. (**I** and **J**) The ratio of TG to cholesterol was calculated in chylomicron (**I**) and VLDL/IDL/LDL (**J**) fractions. (**K**–**M**) TG (**K**), cholesterol (**L**), and PC (**M**) concentration in apoB-containing lipoproteins precipitated from plasma of wild type and LPCAT3-deficient mice (n = 3). Values were normalized to apoB to estimate the amount of each component per particle. See also ***Figure 10—figure supplement 1***.

DOI: 10.7554/eLife.06328.026

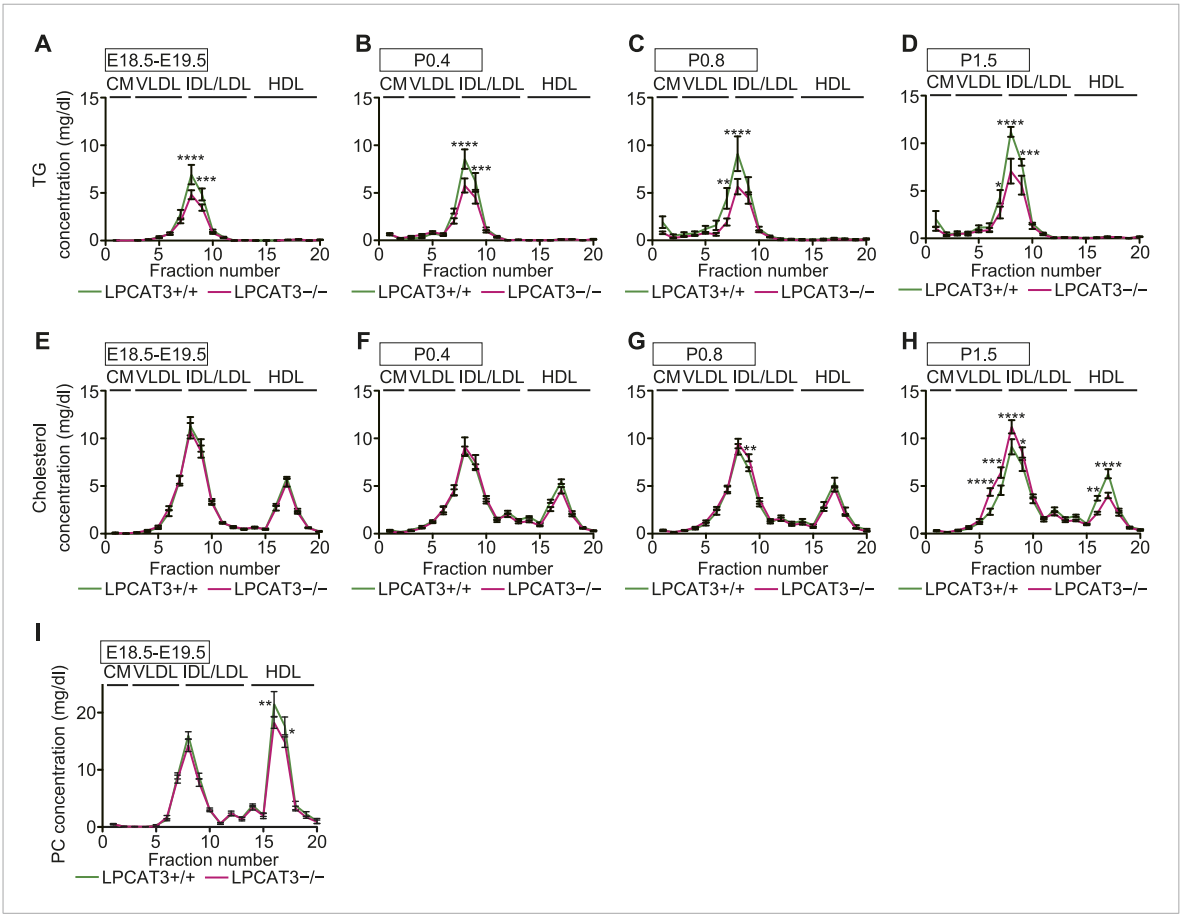

Figure 10—figure supplement 1. Fractionation of plasma lipoproteins by gel-filtration chromatography. Plasma lipoproteins were fractionated by gel-filtration chromatography (n = 5). (**A**–**H**) TG and cholesterol concentrations were analyzed in plasma lipoprotein subfractions from wild type and LPCAT3-deficient mice at E18.5–E19.5 (**A** and **E**), P0.4 (**B** and **F**), P0.8 (**C** and **G**), P1.5 (**D** and **H**). The data are raw data used for calculations in ***Figure 9E–J***. (**I**) PC concentration in plasma lipoprotein subfractions of wild type and LPCAT3-deficient mice at E18.5–E19.5. The annotation of fractions is based on the elution profile of a control plasma. CM: chylomicron; HDL: high-density lipoproteins. Error bars are SEM. *p < 0.05, **p < 0.01, ***p < 0.001, ****p < 0.0001.

DOI: 10.7554/eLife.06328.027

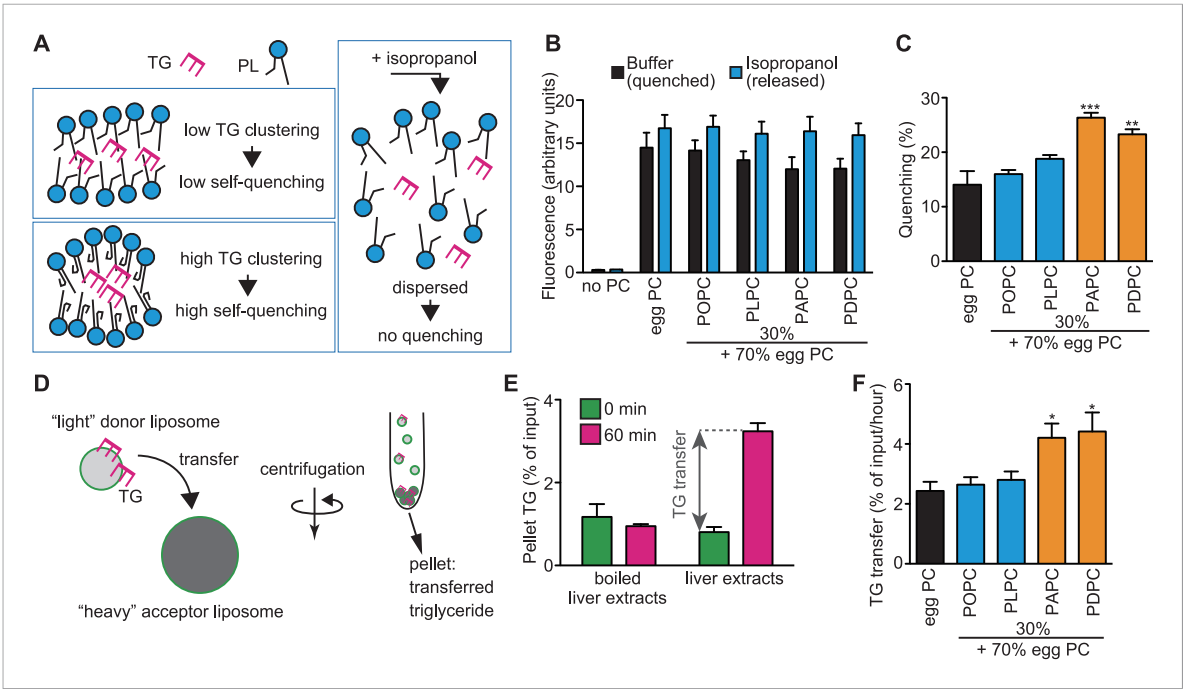

Figure 11. A PUFA-rich membrane promotes TG clustering and efficient transfer. (**A**) Outline of TG clustering analysis based on fluorescence quenching. When TG clustering is higher, quenching increases and fluorescence decreases. Isopropanol disrupts liposomes and TG clustering, leading to fluorescence without quenching. (**B** and **C**) Fluorescence (**B**) and the quenching rate (**C**) of NBD-TG were analyzed in PC liposomes of different compositions. (**D**) Outline of the MTP assay, measuring the transfer of NBD-TG from 'light' donor liposomes to 'heavy' acceptor liposomes. 'Heavy' acceptor liposomes are prepared in the presence of sucrose, and can be pelleted by centrifugation. (**E**) Fluorescence of NBD-TG in acceptor liposomes, after incubation for the indicated time with donor liposomes and liver extracts (or boiled extracts). NBD-TG is transferred to acceptor liposomes after incubation with liver extracts for 1 hr. The difference is used for calculation of TG transfer efficiency. (**F**) TG transfer efficiency was measured using donor PC liposomes of different compositions. Error bars are SEM (n = 3). *p < 0.05, **p < 0.01, ***p < 0.001. See also ***Figure 11—figure supplements 1, 2***.
DOI: 10.7554/eLife.06328.028

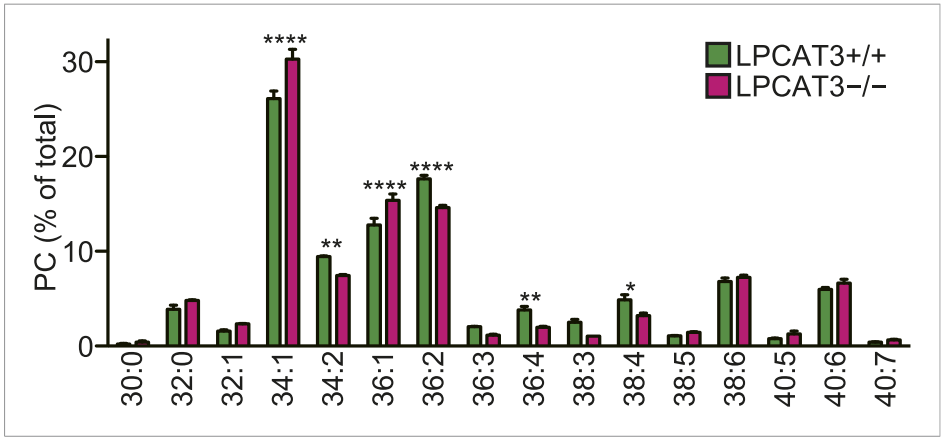

Figure 11—figure supplement 1. PC acyl-chain composition of lipoproteins. PC acyl-chain composition of apoB-containing lipoproteins precipitated from plasma of wild type and LPCAT3-deficient mice at E18.5–E19.5 (n = 3). Note that the major species can be estimated to contain at least one monounsaturated fatty acid (e.g., 16:0–18:1 for 34:1 PC, 18:0–18:1 for 36:1 PC, and 18:1–18:1 for 36:2 PC), and that species that might contain arachidonate (36:4 PC and 38:4 PC) are minor. Error bars are SEM.
DOI: 10.7554/eLife.06328.029

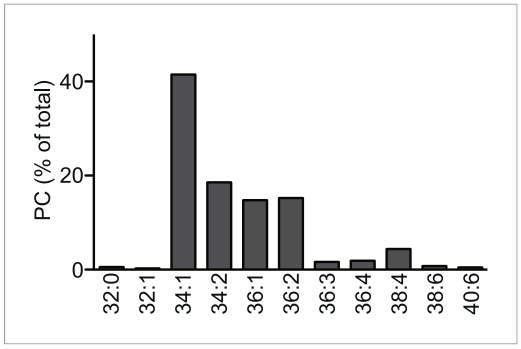

Figure 11—figure supplement 2. Acyl-chain composition of egg PC. Acyl-chain composition of egg PC used in the TG clustering and TG transfer assays (single experiment). Species containing PUFAs are minor.

DOI: 10.7554/eLife.06328.030

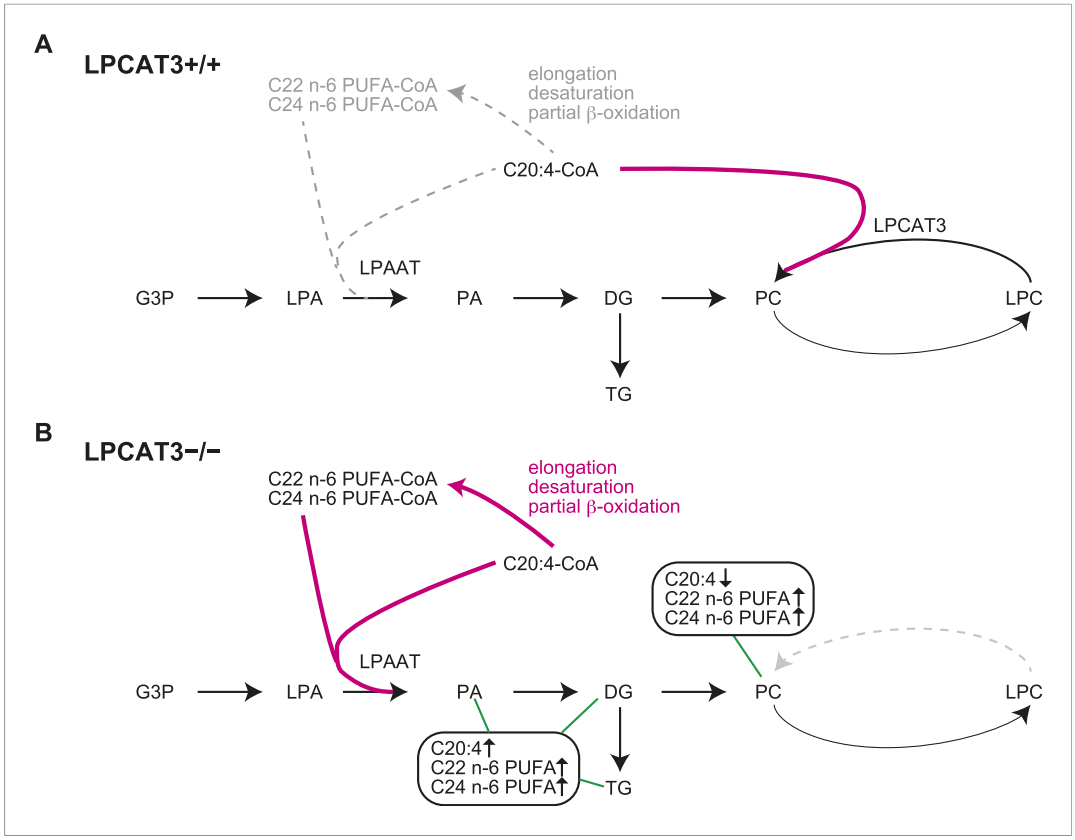

Figure 12. Proposed model of arachidonoyl-CoA shunting in LPCAT3-deficient mice. During de novo synthesis, TG and PC share the same precursor, diacylglycerol (DG). Therefore, the fatty acid profile of neutral lipids is suggestive of incorporation during de novo synthesis of both TG and phospholipids, assuming that TG has a negligible degree of acyl-chain remodeling. Based on the enzymatic assays and the fatty acid profiles of phospholipids and neutral lipids, we propose the following explanation for the results. (**A**) In wild type mice, arachidonoyl-CoA is largely utilized by LPCAT3 to be incorporated into phospholipids. (**B**) In LPCAT3-deficient mice, an excess of arachidonoyl-CoA occurs, which is utilized by LPAATs for de novo synthesis of both phospholipids and triglycerides, either directly or after being metabolized into C22 and C24 n-6 PUFAs (***Figure 3—figure supplement 2***). This pathway is less utilized in wild type mice. The monoacylglycerol acyltransferase pathway of TG synthesis is ignored in this figure, since differences in TG profiles should originate from those synthesized by the embryo and not those provided by the mother bloodstream. G3P: glycerol 3-phosphate; LPA: lysophosphatidic acid; PA: phosphatidic acid.

DOI: 10.7554/eLife.06328.031

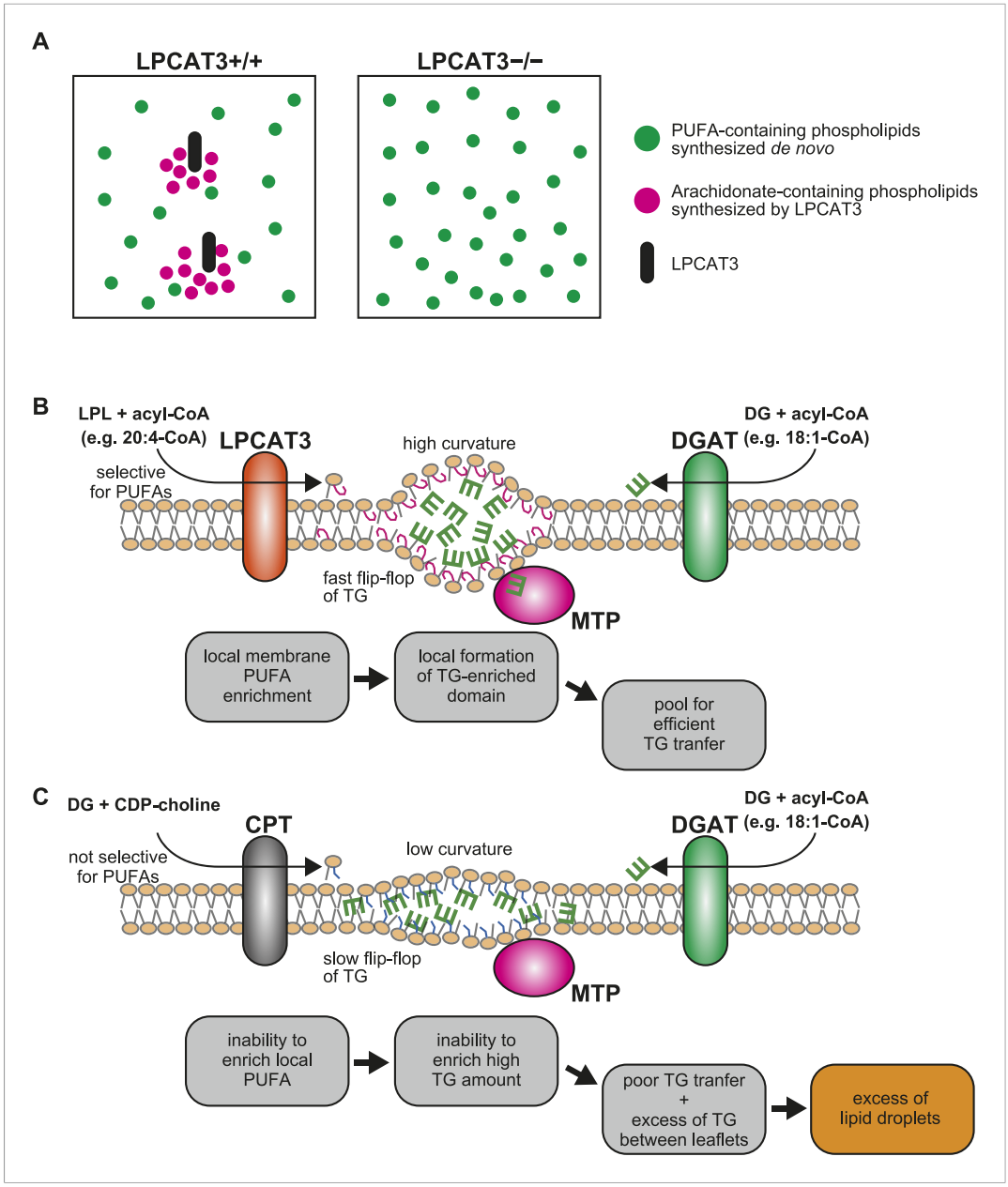

Figure 13. A proposed mechanism of TG transport facilitated by LPCAT3. (**A**) Differences in PUFA-containing phospholipids distribution between wild type and LPCAT3-deficient mice. Since PUFAs are shunted into de novo synthesis (***Figure 12***), the total levels of PUFAs are similar in both genotypes. However, since the remodeling by LPCAT3 is highly selective for arachidonate, arachidonate-containing phospholipids are concentrated around LPCAT3, generating a local membrane area rich in PUFAs. (**B** and **C**) Proposed mechanism of TG transport facilitated by LPCAT3. (**B**) LPCAT3 locally enriches PUFA-containing phospholipids. When TG synthesis occurs in the proximity, this PUFA-enriched domain favors the formation of a blister-like structure with a high capacity and high surface curvature. TG in the blister-like structure has a high flip-flop rate, enabling efficient supply to MTP at the luminal side. (**C**) The substrate selectivity of the final step of PC synthesis does not favor the generation of a PUFA-enriched domain. LPL: lysophospholipid; DG: diacylglycerol; DGAT: diacylglycerol acyltransferase; CPT: diacylglycerol cholinephosphotransferase.

DOI: 10.7554/eLife.06328.032